Cell Reports, Volume *37*

Supplemental information

Cdc42 activity in Sertoli cells is essential for maintenance of spermatogenesis

Anna Heinrich, Bidur Bhandary, Sarah J. Potter, Nancy Ratner, and Tony DeFalco

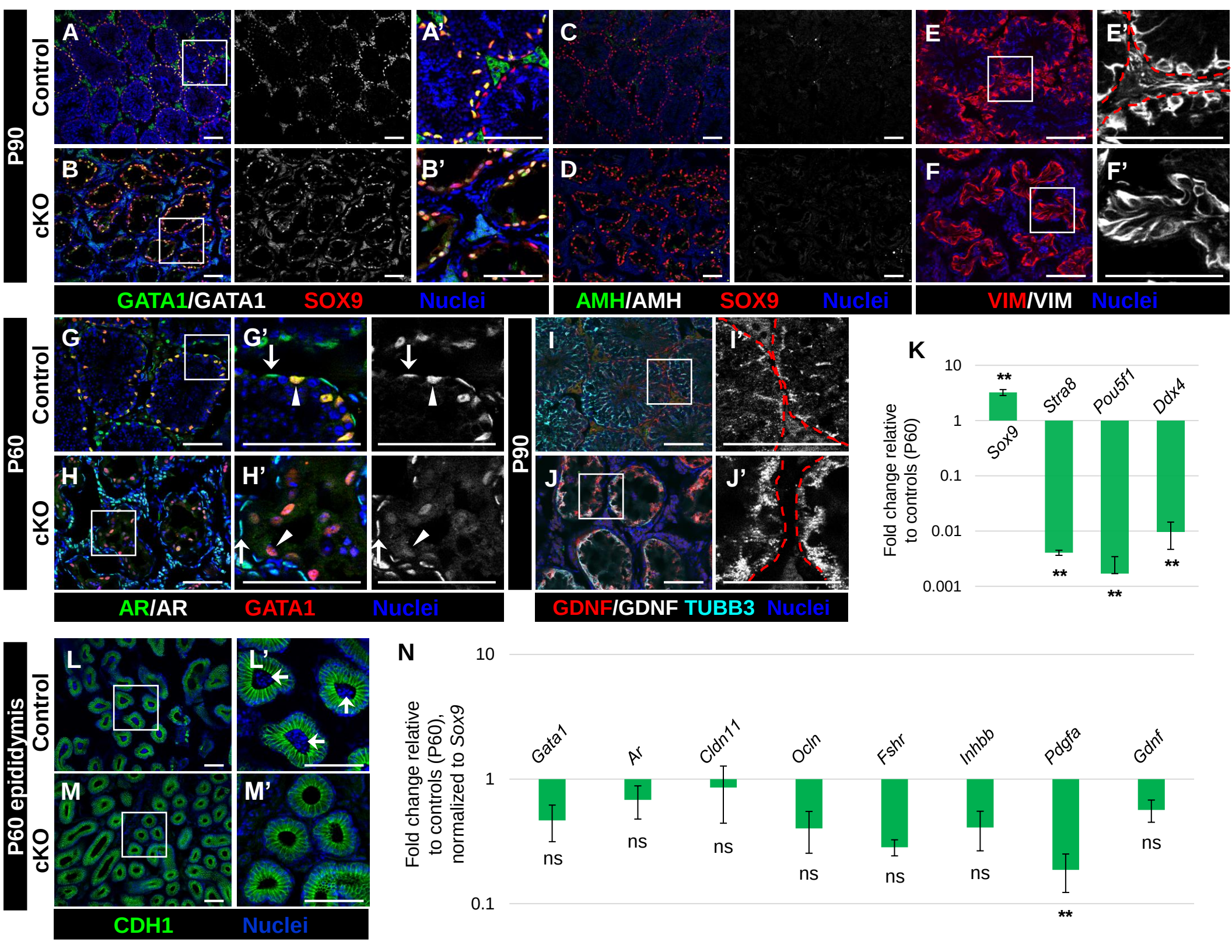
P90
Control
cKO
A
A'
B
B'
C
D
E
E'
F
F'
GATA1/GATA1 SOX9 Nuclei
AMH/AMH SOX9 Nuclei
VIM/VIM Nuclei
P60
G
G'
H
H'
AR/AR GATA1 Nuclei
P90
I
I'
J
J'
GDNF/GDNF TUBB3 Nuclei
K
Fold change relative to controls (P60)
10
1
0.1
0.01
0.001
Sox9
Stra8
Pou5f1
Ddx4
**
P60 epididymis
L
L'
M
M'
CDH1 Nuclei
N
Fold change relative to controls (P60), normalized to Sox9
10
1
0.1
Gata1
Ar
Cldn11
Ocln
Fshr
Inhbb
Pdgfa
Gdnf
ns
**

Figure S1. Loss of *Cdc42* disrupts development of adult Sertoli cells, Related to Figure 1.

(A-J) Immunofluorescence images of adult P90 (A-F,I-J) and P60 (G and H) control *Dhh*-Cre;*Cdc42*$^{flox/+}$ (A,C,E,G,I) and cKO (*Dhh*-Cre;*Cdc42*$^{flox/flox}$) (B,D,F,H,J) testes, and P60 control (L) and cKO (M) epididymis. A', B', E'-J', L' and M' are higher-magnification images of the boxed regions in A, B, E-J, L and M. Dashed lines indicate tubule boundaries. (A and B) Relative to controls (A), Sertoli cells in cKO (B) testes show robust SOX9 expression but heterogeneous GATA1 expression. (C and D) Both control (C) and cKO (D) adult Sertoli cells do not express AMH. (E and F) Control (E) Sertoli cells show specific basal localization of VIM, but cKO (F) cells show diffuse VIM localization throughout the entire cell. (G and H) Control (G) testes show strong nuclear localization of AR in Sertoli cells (arrowhead in G') and peritubular myoid cells (arrow in G'); in contrast, cKO (H) Sertoli cells have diffuse cytoplasmic and weak nuclear AR localization (arrowhead in H'); however, cKO testes have normal nuclear AR localization in peritubular myoid cells (arrow in H'). (I and J) Both control (I) and cKO (J) Sertoli cells exhibit robust GDNF expression. (K) qRT-PCR analyses of whole P60 *Dhh*-Cre;*Cdc42*$^{flox/+}$ control versus cKO testes (n=4 testes for controls and n=3-4 testes for cKO, all from independent males), normalized to *Gapdh*. *Sox9* showed increased relative expression in cKO testes, while germ-cell-expressed genes (*Stra8*, *Pou5f1*, and *Ddx4*) showed dramatically reduced expression in cKO testes. (L and M) Whereas P60 control (L) epididymal lumina contain sperm (as detected by nuclear dye staining; arrows in L'), cKO (M) epididymal lumina are devoid of sperm. (N) qRT-PCR analyses of whole P60 *Dhh*-Cre;*Cdc42*$^{flox/+}$ control versus cKO testes (n=4 testes for controls and n=3-4 testes for cKO, all from independent males), focused on Sertoli-expressed genes. Data in N are additionally normalized to *Sox9* to account for an increased relative proportion of Sertoli cells in germ-cell-depleted cKO testes. Data in K and N are shown as mean fold change ± SD. **, $P<0.01$; ns, not significant ($P>0.05$). *P* values were calculated via a two-tailed Student t-test. Scale bars, 100 μm.

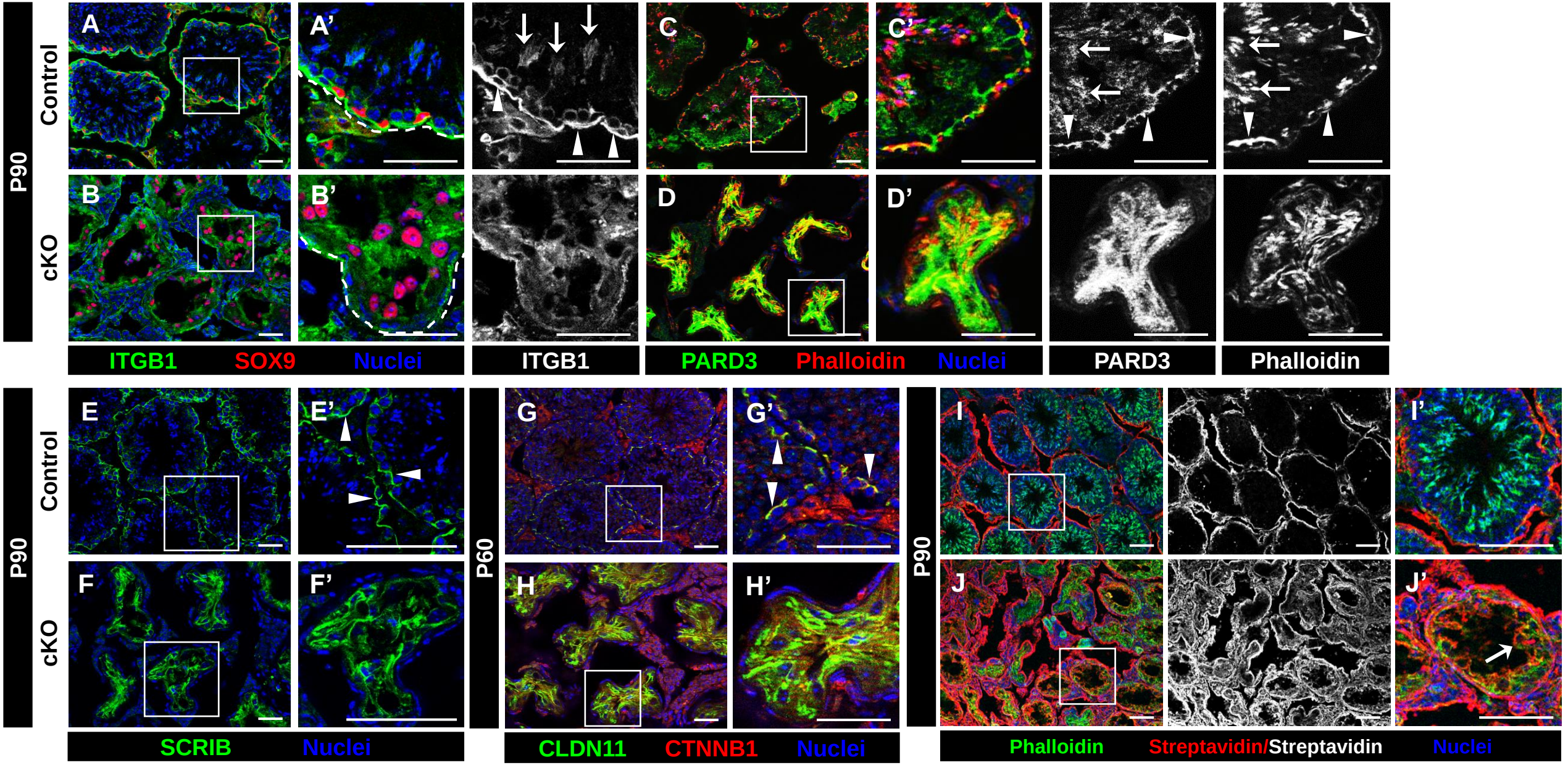
P90
Control
cKO
A
A'
B
B'
C
C'
D
D'
ITGB1
SOX9
Nuclei
ITGB1
PARD3
Phalloidin
Nuclei
PARD3
Phalloidin
P90
Control
cKO
E
E'
F
F'
SCRIB
Nuclei
P60
G
G'
H
H'
CLDN11
CTNNB1
Nuclei
P90
I
I'
J
J'
Phalloidin
Streptavidin/Streptavidin
Nuclei

Figure S2. *Cdc42* activity is required for proper localization of polarity protein complexes and BTB integrity in adult testes, Related to Figure 1.

Immunofluorescence images of adult P90 (A-F,I,J) and P60 (G and H) control *Dhh*-Cre;*Cdc42*$^{flox/+}$ (A,C,E,G,I) and cKO (B,D,F,H,J) testes. A'-J' are higher-magnification images of the boxed regions in A-J. Dashed lines indicate tubule boundaries. (A-D) In control (A and C) tubules, ITGB1, PARD3, and F-actin (via phalloidin) are enriched in the apical ES (arrows in A' and C') and basally in the BTB or basement membrane (arrowheads in A' and C'), but in cKO (B and D) tubules these proteins are diffusely localized. (E and F) Control tubules (E) display specific SCRIB localization in the basal compartment (arrowheads in E'), but cKO (F) tubules exhibit diffuse SCRIB localization. (G and H) In control (G) testes, CLDN11 and CTNNB1 are enriched in the BTB (arrowheads in G') but are localized throughout entire cKO (H) tubules. (I and J) Biotin tracer injections into P90 control (I) testes reveal biotin presence only in the interstitium and basal-most tubule cells, but in P90 cKO (J) testes there is widespread, deep penetration of biotin near tubule lumina (arrow in J'). Scale bars, 50 μm.

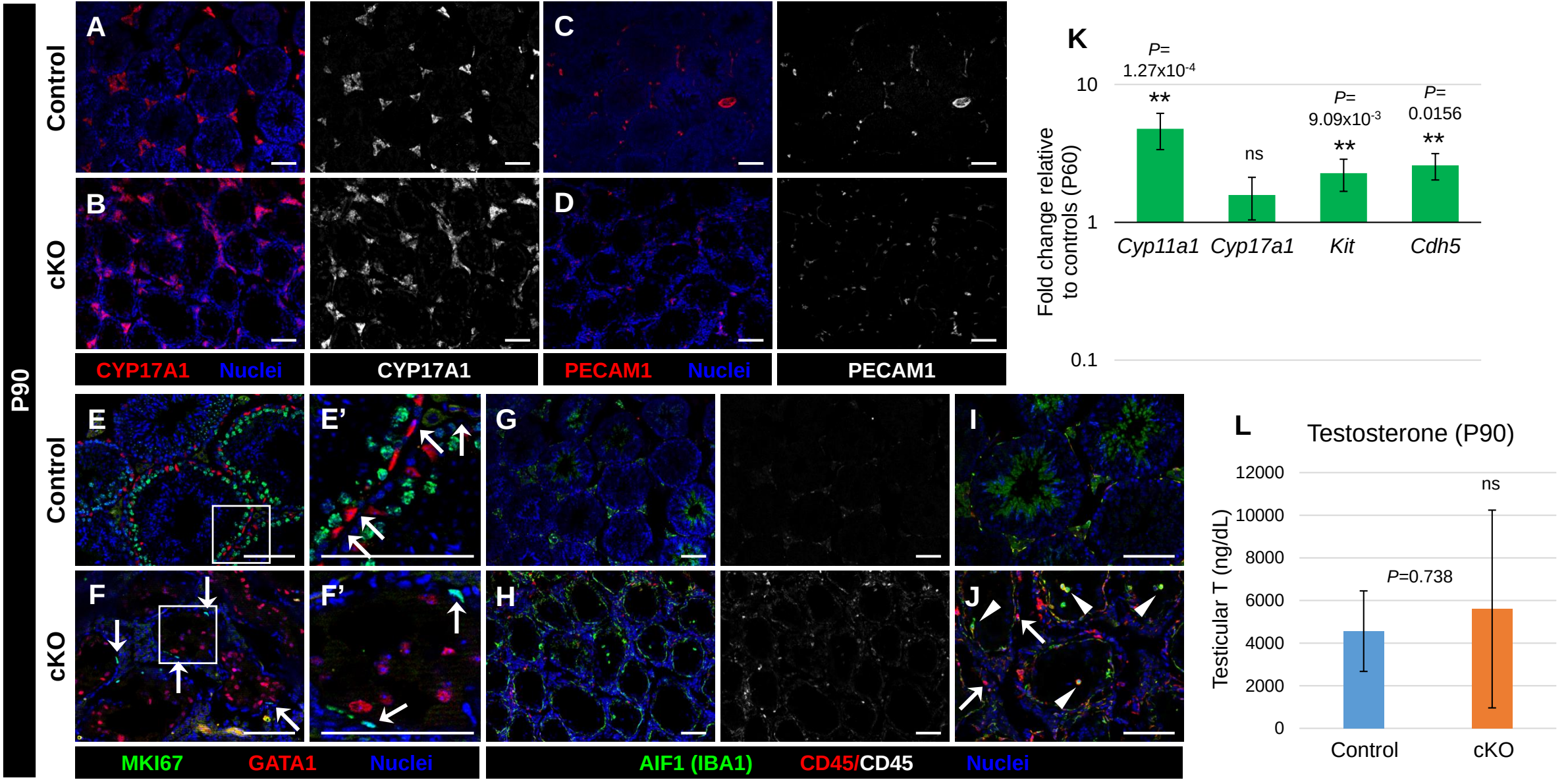
P90
Control
cKO
A
B
C
D
CYP17A1 Nuclei
CYP17A1
PECAM1 Nuclei
PECAM1
K
P= 1.27x10-4
P= 9.09x10-3
P= 0.0156
**
ns
**
**
10
1
0.1
Fold change relative to controls (P60)
Cyp11a1
Cyp17a1
Kit
Cdh5
E
E'
F
F'
G
H
I
J
MKI67 GATA1 Nuclei
AIF1 (IBA1) CD45/CD45 Nuclei
L
Testosterone (P90)
Testicular T (ng/dL)
12000
10000
8000
6000
4000
2000
0
P=0.738
ns
Control
cKO

Figure S3. Adult cKO testes show normal development and function of the interstitial compartment, Related to Figure 1.

(A-J) Immunofluorescence images of adult P90 control *Dhh*-Cre;*Cdc42*$^{flox/+}$ (A,C,E,G,I) and cKO (B,D,F,H,J) testes. E' and F' are higher-magnification images of the boxed regions in E and F. (A and B) Compared to controls (A), cKO (B) testes contain similarly abundant CYP17A1+ Leydig cells in the interstitium. (C and D) Both control (C) and cKO (D) testes display extensive vascularization (PECAM1+ cells). (E and F) Relative to control (E) testes, cKO (F) testes show increased MKI67 immunoreactivity in interstitial cells such as peritubular myoid cells (arrows in E' and F'). (G-J) While control (G and I) testes have CD45+ immune cells, such as macrophages (AIF1+), in the interstitium, cKO (H and J) testes exhibit increased CD45-bright immune cell infiltration (likely T cells; arrows in J) in the interstitium, as well as ectopic macrophage presence within tubule lumina (arrowheads in J). Scale bars, 100 µm. (K) qRT-PCR analyses of interstitial gene expression in P60 adult cKO testes relative to control *Dhh*-Cre;*Cdc42*$^{flox/+}$ testes (n=4 testes for controls and n=3-4 testes for cKO, all from independent males). *Cyp11a1* and *Cyp17a1* are specific to Leydig cells; *Kit* is expressed in Leydig cells and differentiating spermatogonia; and *Cdh5* is specific to vascular endothelial cells. (L) Graph showing levels of testosterone in testicular homogenate of control *Dhh*-Cre;*Cdc42*$^{flox/+}$ versus cKO mice (n=3 testes each for controls and cKO, all from independent males). Data in K and L are shown as mean ± SD. *P* values were calculated via a two-tailed Student t-test. **, $P<0.01$; ns, not significant ($P>0.05$).

A

Fetal expression (by stage and cell type)
(Jameson et al., 2012)

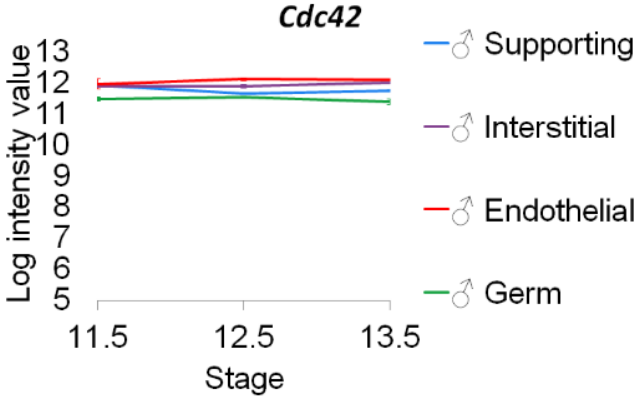

B

Fetal *Cdc42* expression (by stage)
(Stevant et al., 2018)

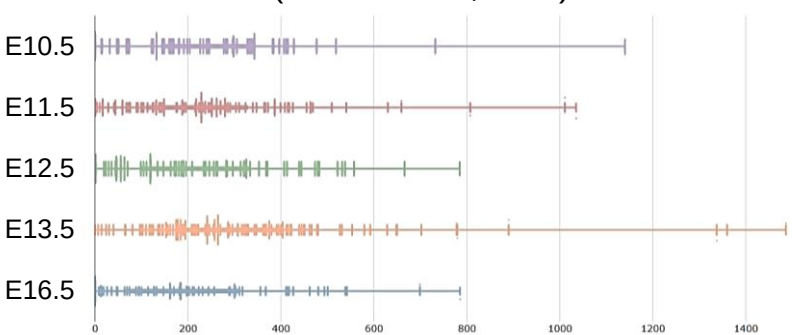

C

Fetal *Cdc42* expression (by cell type)
(Stevant et al., 2018)

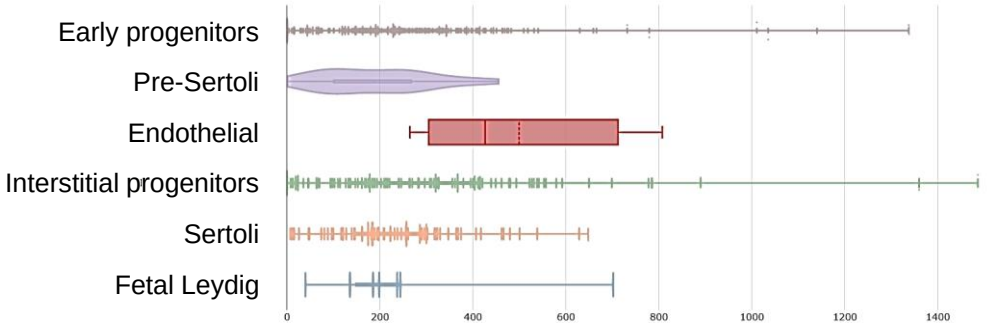

D

Adult *Cdc42* expression (by cell type)
(Green et al., 2018)

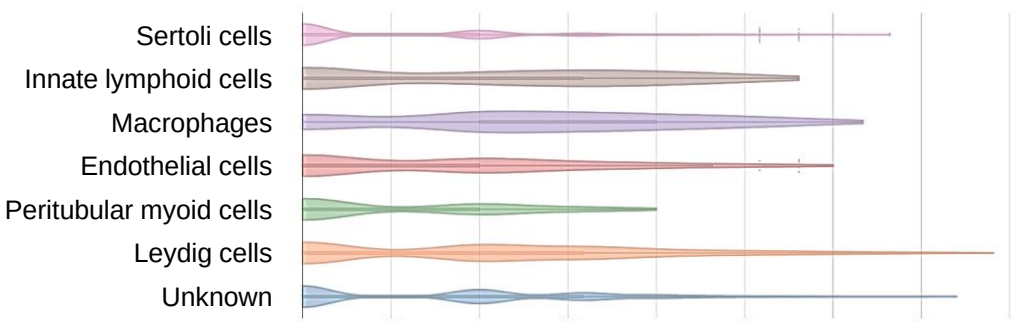

Figure S4. *Cdc42* is expressed in Sertoli cells throughout fetal development and during adulthood, Related to Figure 2.

(A) Plot showing *Cdc42* expression levels, which were generated from fetal gonad cell-type-specific microarray data (Jameson et al., 2012), where cell types (i.e., supporting Sertoli cells, interstitial cells, endothelial cells, and germ cells) were each plotted in different colors. Plot shows expression levels for each cell type in E11.5, E12.5, and E13.5 XY gonads. Expression values below 6 are generally considered background expression. *Cdc42* is expressed at high levels in all cell types throughout all 3 stages. (B-D) Violin plots showing single-cell RNA-Seq data for fetal (B and C) and adult (D) testes, from previously published datasets (Green et al., 2018; Stevant et al., 2018), showing *Cdc42* expression plotted by either stage (B) or cell type (C and D). Plots in B-D were generated using The ReproGenomics Viewer (Darde et al., 2019; Darde et al., 2015).

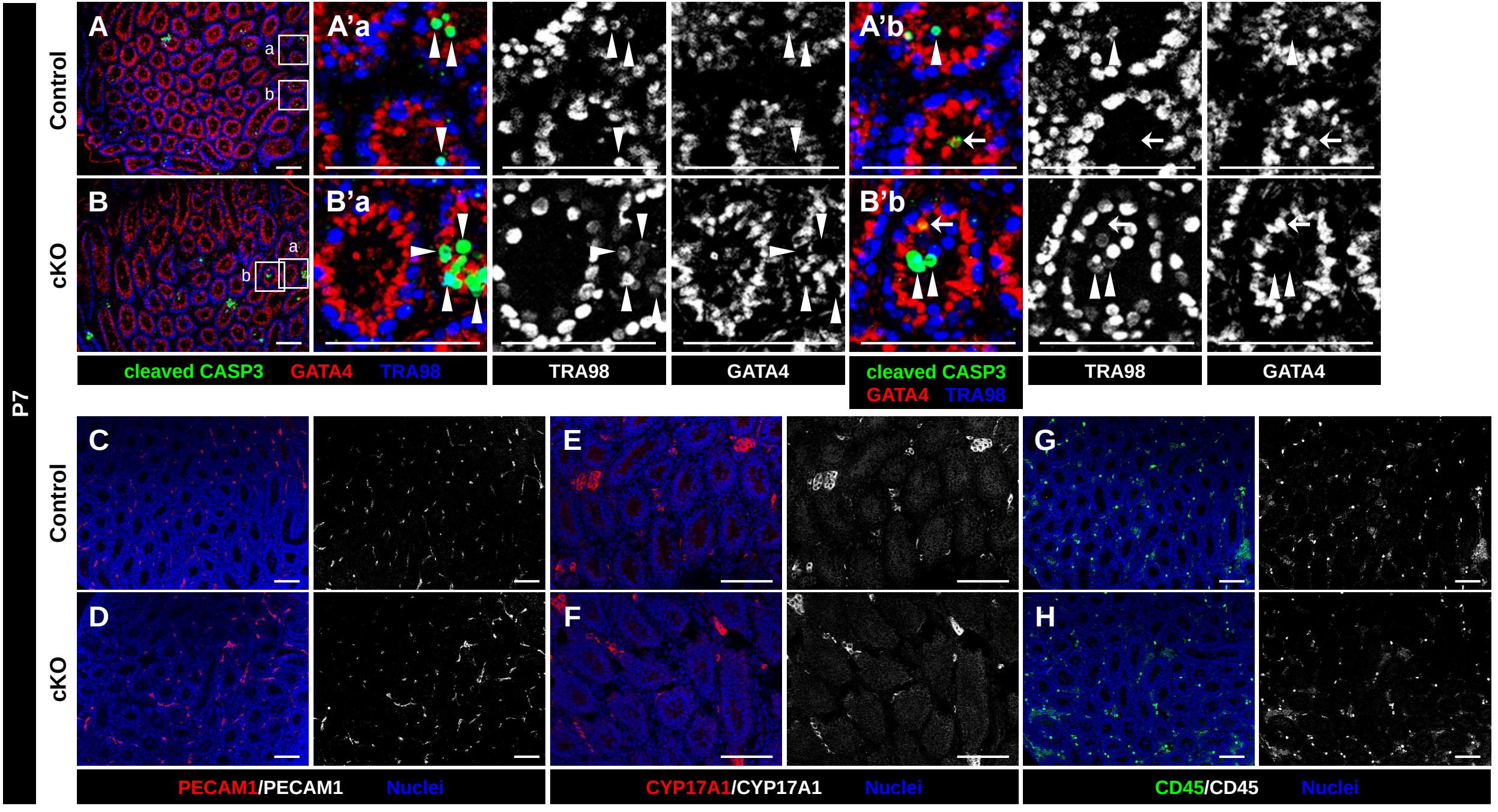
P7
Control
cKO
A
A'a
A'b
B
B'a
B'b
a
b
cleaved CASP3 GATA4 TRA98
TRA98
GATA4
cleaved CASP3
GATA4 TRA98
TRA98
GATA4
C
D
E
F
G
H
PECAM1/PECAM1 Nuclei
CYP17A1/CYP17A1 Nuclei
CD45/CD45 Nuclei

Figure S5. Levels of apoptosis and development of the interstitial compartment are normal in early postnatal cKO testes, Related to Figure 3.

Immunofluorescent images of P7 control *Dhh*-Cre;*Cdc42*$^{flox/+}$ (A,C,E,G) and cKO (B,D,F,H) testes. A'a, A'b, B'a, and B'b are higher-magnification images of the corresponding labeled boxed regions in A and B. (A and B) Similar levels of cleaved caspase 3-positive apoptotic cells are observed in control (A) and cKO (B) testes; co-stains indicate most apoptotic cells are germ cells (arrowheads in A'a, A'b', B'a, and B'b) with Sertoli cells less often detected undergoing cell death (arrows in A'b' and B'b). (C and D) Both control (C) and cKO (D) testes exhibit extensive interstitial vascularization by PECAM1+ endothelial cells. (E and F) Similar to controls (E), cKO (F) testes contain interstitial CYP17A1+ Leydig cells. (G and H) No gross differences are observed in overall cell number of CD45+ immune cells in control (G) versus cKO (H) testes. Scale bars, 100 μm.

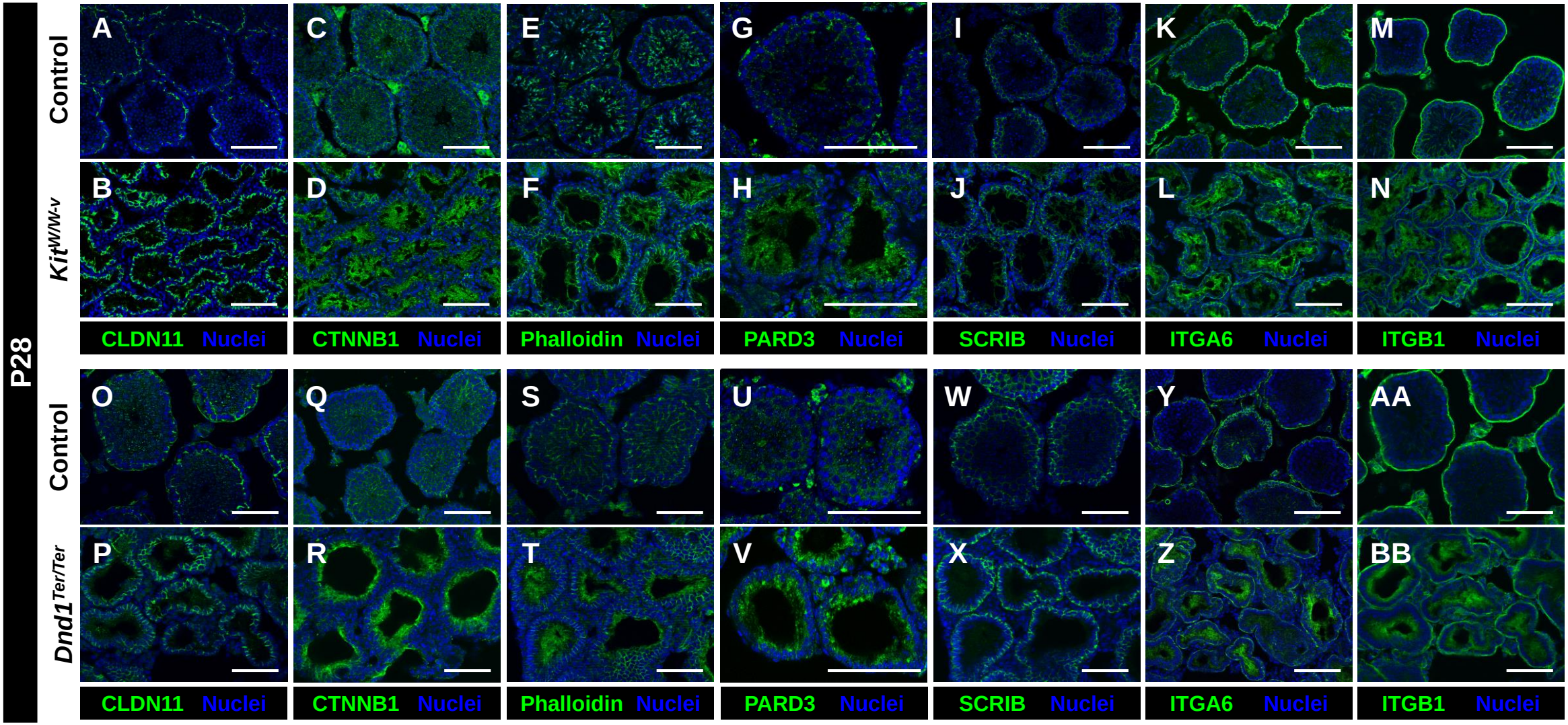
P28
Control
Kit W/W-v
Control
Dnd1 Ter/Ter
A
B
C
D
E
F
G
H
I
J
K
L
M
N
O
P
Q
R
S
T
U
V
W
X
Y
Z
AA
BB
CLDN11 Nuclei
CTNNB1 Nuclei
Phalloidin Nuclei
PARD3 Nuclei
SCRIB Nuclei
ITGA6 Nuclei
ITGB1 Nuclei

Figure S6. Expression and localization of cell polarity factors in juvenile testes of mouse genetic models of germ cell depletion, Related to Figure 6.

Immunofluorescent images of polarity complex proteins, phalloidin, and integrins in P28 control (mixed background of WB/ReJ and C57BL/6J) (A,C,E,G,I,K,M), *Kit*$^{W/W\text{-}v}$ mutant (B,D,F,H,J,L,N), control (*Dnd1*$^{Ter/+}$) (O,Q,S,U,W,Y,AA), and *Dnd1*$^{Ter/Ter}$ mutant (P,R,T,V,X,Z,BB) juvenile testes. Both models show similar phenotypes with respect to changes in cell polarity markers, in that CLDN11 localization (A,B,O,P), basal phalloidin staining (E,F,S,T), and SCRIB localization (I,J,W,X) were unaffected in mutant testes, while CTNBB1 (C,D,Q,R), PARD3 (G,H,U,V), and integrins (K-N,Y-BB) were aberrantly localized in mutant testes. Scale bars, 100 μm.

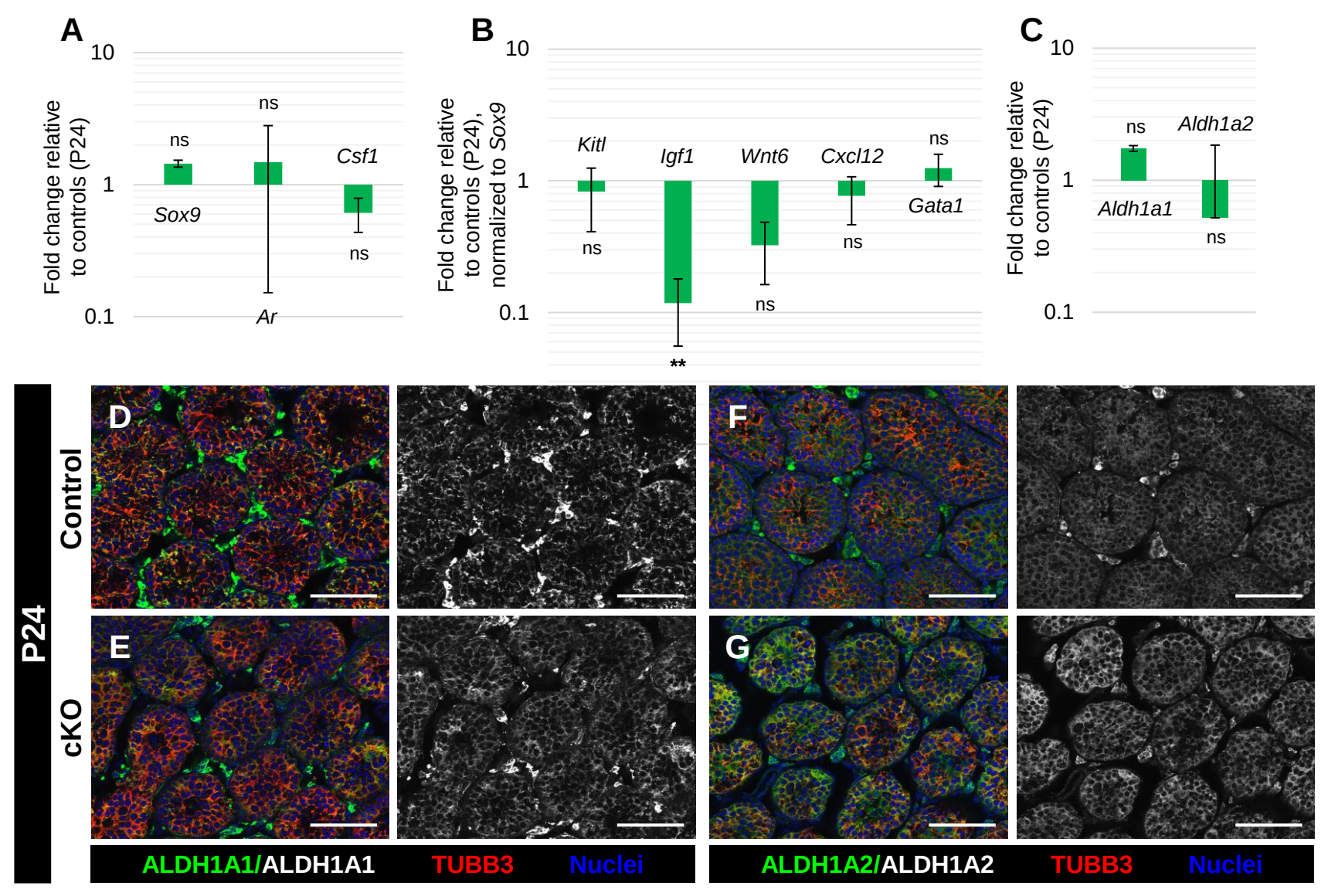
A
B
C
Fold change relative to controls (P24)
Fold change relative to controls (P24), normalized to Sox9
10
1
0.1
ns
Sox9
Ar
Csf1
Kitl
Igf1
Wnt6
Cxcl12
Gata1
**
Aldh1a1
Aldh1a2
P24
Control
cKO
D
E
F
G
ALDH1A1/ALDH1A1
TUBB3
Nuclei
ALDH1A2/ALDH1A2
TUBB3
Nuclei

Figure S7. Expression of factors involved in SSC maintenance and RA synthesis in juvenile cKO testes, Related to Figure 7.

(A-C) qRT-PCR analyses showing expression fold changes in Sertoli-specific and testicular expressed genes associated with testicular function and SSC maintenance (A and B) and genes encoding RA synthesis enzymes (C) in whole P24 cKO testes versus controls (n=3-4 testes each for controls and cKO, all from independent males). Analyses in B include additional normalization to *Sox9* for Sertoli-expressed genes to account for any changes in the proportion of Sertoli cells to whole testicular cells after a decrease in germ cell numbers in P24 cKO testes. Data in A-C are shown as mean ± SD. *P* values were calculated via a two-tailed Student t-test. **, $P<0.01$; ns, not significant ($P>0.05$). (D-G) Immunofluorescent images of P24 control (D and F) and cKO (E and G) testes for RA synthesis enzymes ALDH1A1 and ALDH1A2, showing robust expression in cKO testes. Scale bars, 100 µm.

Table S1. Primers used for qRT-PCR analyses, Related to STAR Methods.

Sequences of primers used for quantitative real-time PCR (qRT-PCR) in this study (in alphabetical order).

Gene name	Sequence (5' to 3')
Aldh1a1 forward	CTCCTCTCACGGCTCTTCAC
Aldh1a1 reverse	CCATGGTGTGCAAACTCAAC
Aldh1a2 forward	ATGGGTGAGTTTGGCTTACG
Aldh1a2 reverse	GGTTCATTGGAAGGCAGAAA
Amh forward	CCACACCTCTCTCCACTGGTA
Amh reverse	GGCACAAAGGTTCAGGGGG
Ar forward	CAGGAGGTAATCTCCGAAGGC
Ar reverse	ACAGACACTGCTTTACACAACTC
Cdh5 forward	TCCTCTGCATCCTCACTATCACA
Cdh5 reverse	GTAAGTGACCAACTGCTCGTGAAT
Cldn11 forward	ATGGTAGCCACTTGCCTTCAG
Cldn11 reverse	AGTTCGTCCATTTTTCGGCAG
Csf1 forward	TTGCCAAGGAGGTGTCAGAACACT
Csf1 reverse	AAGGCAATCTGGCATGAAGTCTCC
Cxcl12 forward	TGCATCAGTGACGGTAAACCA
Cxcl12 reverse	TTCTTCAGCCGTGCAACAATC
Cyp11a1 forward	GGAGGAAGCCGACAACAATGA
Cyp11a1 reverse	TCCACCTCACACGGTTCTCAA
Cyp17a1 forward	CAGAGAAGTGCTCGTGAAGAAG
Cyp17a1 reverse	AGGAGCTACTACTATCCGCAAA
Ddx4 forward	TACTGTCAGACGCTCAACAGGA
Ddx4 reverse	ATTCAACGTGTGCTTGCCCT
Fshr forward	GGGATCTGGATGTCATCACT
Fshr reverse	GGAGAACACATCTGCCTCTA
Gapdh forward	AGGTCGGTGTGAACGGATTTG
Gapdh reverse	TGTAGACCATGTAGTTGAGGTCA
Gata1 forward	TGGGGACCTCAGAACCCTTG
Gata1 reverse	GGCTGCATTTGGGGAAGTG
Gdnf forward	GACTTGGGTTTGGGCTATGA
Gdnf reverse	AACATGCCTGGCCTACTTTG
Igf1 forward	CTGGACCAGAGACCCTTTGC
Igf1 reverse	GGACGGGGACTTCTGAGTCTT
Inhbb forward	GAGCGCGTCTCCGAGATCATCA
Inhbb reverse	CGTACCTTCCTCCTGCTGCCCTT
Kit forward	CATGGCGTTCCTCGCCT
Kit reverse	GCCCGAAATCGCAAATCTTT
Kitl forward	CTATCTGCAGCCGCTGCTGG
Kitl reverse	CTGTTACCAGCCACTGTGCG
Pdgfa forward	GACGGTCATTTACGAGATACCTC
Pdgfa reverse	CTACGCCTTCCTGTCTCCTC
Pou5f1 forward	GGAGGAAGCCGACAACAATGA
Pou5f1 reverse	TCCACCTCACACGGTTCTCAA
Sox9 forward	GCGGAGCTCAGCAAGACTCTG
Sox9 reverse	ATCGGGGTGGTCTTTCTTGTG
Stra8 forward	GCAGGTTGAAGGATGCTTTGAGC
Stra8 reverse	CCTAAGGAAGGCAGTTTACTCCCAGTC
Wnt6 forward	AATGAATTCTCCCGCCTCGGACTGCTGCTGC
Wnt6 reverse	GAATTCTCTGCGCACCTGCTGGCAGAA

SUPPLEMENTAL MOVIES

Movie S1. Three-dimensional imaging of actin cytoskeletal structure in P24 control tubule, Related to Figure 6.

Movie showing three-dimensional imaging of a P24 control (*Dhh*-Cre;*Cdc42*$^{flox/+}$) seminiferous tubule stained for phalloidin, showing the enrichment of the actin cytoskeleton at the blood-testis barrier. The 3D reconstruction is comprised of 20 individual z-sections over a width of 39.5 µm.

Movie S2. Three-dimensional imaging of actin cytoskeletal structure in P24 cKO tubules, Related to Figure 6.

Movie showing three-dimensional imaging of P24 cKO (*Dhh*-Cre;*Cdc42*^{floxflox}) seminiferous tubules stained for phalloidin, showing a lack of actin cytoskeletal enrichment at the blood-testis barrier and overall throughout the tubule. The 3D reconstruction is comprised of 20 individual z-sections over a width of 37.2 µm.